

Phase Coherence and Andreev Reflection in Topological Insulator Devices

A.D.K. Finck^{1*}, C. Kurter^{1*}, Y.S. Hor², D.J. Van Harlingen¹

¹*Department of Physics and Materials Research Laboratory,*

University of Illinois at Urbana-Champaign, Urbana, Illinois 61801

²*Department of Physics, Missouri University of Science and Technology, Rolla, MO 65409*

** These authors contributed equally to the work.*

(Dated: March 25, 2014)

Topological insulators (TIs) have attracted immense interest because they host helical surface states [1]. Protected by time-reversal symmetry, they are robust to non-magnetic disorder. When superconductivity is induced in these helical states, they are predicted to emulate p -wave pairing symmetry, with Majorana states bound to vortices [2]. Majorana bound states possess non-Abelian exchange statistics which can be probed through interferometry [3–8]. Here, we take a significant step towards Majorana interferometry by observing pronounced Fabry-Perot oscillations in a TI sandwiched between a superconducting and normal lead. For energies below the superconducting gap, we observe a doubling in the frequency of the oscillations, arising from the additional phase accumulated from Andreev reflection [9, 10]. When a magnetic field is applied perpendicular to the TI surface, a number of very sharp and gate-tunable conductance peaks appear at or near zero energy, which has consequences for interpreting spectroscopic probes of Majorana fermions [11–15]. Our results demonstrate that TIs are a promising platform for exploring phase-coherent transport in a solid-state system.

When electrons travel far distances without scattering off of impurities, their wave-like nature becomes apparent through signatures of interference. A prominent example is ballistic transmission through a barrier between two semi-infinite leads. Imperfect transmission through the interfaces causes partial reflection of impinging electrons. Within the barrier, constructive interference of reflected waves leads to periodic modulation of total transmission through the barrier, resulting in resonant transmission whenever the electron wavelength is an integer multiple of twice the barrier length. This is equivalent to $k_F L = \pi n$, where k_F is the Fermi wave vector, L is the barrier length, and n is a nonzero integer.

This quantum phenomenon, known as Fabry-Perot interference due to its similarity to the eponymous classical optical effect, has been observed in a variety of mesoscopic systems, including nanotubes [16], nanowires [17], and graphene [18]. In topological systems with protected edge states, interferometry takes on a new significance as particles traveling through the edge states can acquire an additional phase if their paths enclose exotic quasiparticles known as anyons [3]. A class of anyons known as Majorana bound states (MBSs) can be realized in a topological insulator with induced superconductivity [2]. MBSs can encode quantum information non-locally, realizing topologically protected qubits whose states can be read out through interferometry [4–6].

We study Andreev reflection in thin (~ 10 nm) flakes of the 3D topological insulator Bi_2Se_3 connected to both superconducting and normal metal leads separated by $L = 100 - 250$ nm. An example of a device with $L = 230$ nm is pictured in Fig. 1a. Either top or back gates are used to tune the chemical potential of the surface states, depicted in Fig. 1b. Here we focus on one sample, with qualitatively similar results obtained from others (see Supplementary Materials). At low temperature, we observe an enhancement in conductance at source-drain voltages (V) below the niobium gap, as expected for Andreev reflection (Fig. 1c) [19–21]. Near $V = 0$, however, there is a downturn in the conductance. This is consistent with the re-entrant resistance effect [22, 23], in which Andreev reflection is cancelled out by the proximity effect in the limit of zero energy and zero temperature [23, 24]. Maximum conductance occurs at either a characteristic temperature or V that is governed by the Thouless energy $E_T = \hbar D/L^2$, where D is the diffusion constant and L is the separation between the superconducting and normal metal leads on the bismuth selenide. Magnetotransport and ARPES measurements [25] allow us to calculate E_T through $D = \frac{1}{2}v_F l = \frac{1}{2}v_F \mu(\frac{\hbar}{2e})\sqrt{N_{2D}/\pi} \approx 0.0025$ m²/s, where v_F is the Fermi velocity, l is the mean

free path, μ is the mobility, N_{2D} is the 2D carrier density. This results in $E_T = 30 \mu\text{V}$ for $L = 230 \text{ nm}$, consistent with our transport measurements ($T_{max} = 900 \text{ mK}$ and $V_{max} = 85 \mu\text{V}$). At high temperature (Fig. 1d), the conductance dip disappears and only a broad peak from Andreev reflection remains. We note in passing a remarkable similarity between Fig. 1 and the predictions of Ref. [26], which posited that anomalous Andreev bound states on the surface of a topological superconductor would generate an asymmetric zero bias tunneling conductance peak [27] that splits at low temperature. However, we feel that our data is most likely a result of the re-entrant resistance effect. Devices with smaller L possess larger E_T and are observed to have a broader suppression in conductance around zero bias (see Supplementary Materials).

To demonstrate phase coherent transport, we turn to gate-tuned measurements. In Fig. 1e, we display a stability plot of conductance vs V and back gate voltage V_{BG} . At higher bias (Fig. 2a), we observe a checkerboard pattern that is characteristic of Fabry-Perot oscillations. The periodic variation in conductance coexist with aperiodic universal conductance fluctuations (UCFs), which have been previously reported in bismuth selenide [28]. Whenever the Fermi wave vector k_F is tuned to a Fabry-Perot resonance, constructive interference generates enhanced conductance. Shifts in V or V_{BG} will shift the Fermi energy E_F of incident electrons by a proportional amount. With a linear approximation $E_F = \hbar v_F k_F$, one expects subsequent Fabry-Perot resonances to differ in energy by $\Delta E = \frac{\hbar v_F}{2L}$. For $V > \Delta/e$ (upper graph in Fig. 2b), we observe oscillations with period $\Delta E = 0.8 \text{ mV}$. This somewhat disagrees with the estimate 3.8 mV , possibly due to renormalization of the Fermi velocity. Nonetheless, the clear oscillations that we observe represent, to our knowledge, the first demonstration of gate-tuned Fabry-Perot oscillations in a topological insulator. Devices with smaller L are observed to have larger ΔE (Supplementary Materials). Remarkably, such oscillations can be observed without special care for cleanliness, as achieved in other materials through current annealing or isolating the material from dielectric impurities by suspension from the substrate. This is likely due to the topological protection of the helical surface states, although we do not rule out the contribution from trivial states. The peak-to-peak amplitude of the oscillations are $\approx 0.2e^2/h$, independent of normal state resistance, which varies from 600Ω to $21 \text{ k}\Omega$ in our three devices. This suggests that while bulk carriers might contribute to the zero bias conductance, the interference originates from a finite number of surface states.

The most unusual feature of the Fabry-Perot oscillations in Fig. 2 is a doubling of their frequency when V is less than the superconducting gap of niobium, as shown in the lower graph in Fig. 2b. Coulomb repulsion can split otherwise degenerate levels [29], but the high degree of coupling between the leads and the TI should minimize charging effects. Furthermore, the peaks in conductance at low bias are evenly separated in V_{BG} , unlike the uneven spacing expected for split degeneracies. Instead, this behavior can be understood as a modification of phase coherent transport by Andreev reflection. Low energy electrons passing from the cavity to the superconducting lead will be retro-reflected as a hole with high probability in the absence of significant barrier, depicted in the lower cartoon in Fig. 2b. As first pointed out by de Gennes and Saint-James, the reflected hole traverses the cavity and reflects off the interface with the normal metal lead. The holes do not interfere with the incident electrons; instead, the hole returns to the superconducting lead to undergo Andreev reflection again, leading to an emitted electron. This reflected electron can traverse the cavity and subsequently interfere with incident electrons. Because in this process the reflected particles travel four times the cavity length rather than twice the cavity length, the corresponding geometric resonances occur with twice the frequency. Although this interplay between Andreev reflection and geometric resonances was predicted over 50 years ago [9, 10], we believe this to be the first observation of a clear cross-over from de Gennes-Saint-James resonances to conventional Fabry-Perot behavior.

In Fig. 2c, we explore the temperature dependence of the Fabry-Perot oscillations. The amplitude of the oscillations is rapidly suppressed by thermal fluctuations, decreasing by roughly a factor of two between 20 mK and 1.6 K. This is consistent with the temperature dependence of the phase-coherence length l_ϕ from weak anti-localization measurements in Hall bar devices, helping to confirm that the oscillations are an interference phenomenon.

We next consider transport in magnetic fields applied perpendicular to the TI surface. While in-plane fields have no influence up to at least 100 mT, with out-of-plane fields we observe a steady evolution of the background signal from universal conductance fluctuations and suppression of superconductivity, as shown in Fig. 2d. While the amplitude of the Fabry-Perot oscillations are similarly reduced, their phase does not change appreciably, suggesting that the fields we use are too small to observe the phase shift expected from Klein backscattering [30]. Small shifts can be observed in the features from Fabry-Perot oscillations, but it is difficult to reliably disentangle them from the evolving background

signal due to universal conductance fluctuations.

Strikingly, in two of our samples we observe a number of narrow, low energy conductance peaks emerge at large magnetic fields. An example is shown in Fig. 3a, with data from the second device shown in the Supplementary Materials. The location of the peaks can be tuned readily with V_{BG} , causing them to even form a zero bias conductance peak for certain gate ranges with height $\approx e^2/h$, indicated in Fig. 3b. The peaks split and reform in a quasi-periodic fashion that does not seem to be directly related to the Fabry-Perot oscillation period. In Fig. 4a, we detail the field evolution of one of these zero bias anomalies. We find that the zero energy resonance forms at finite field and can persist for at least up to 120 mT. At elevated temperatures (Fig. 4b), we find these anomalies broaden and merge with the background.

These peaks are notable because no such features are seen in these two samples at zero magnetic field. They appear only when large fields are applied perpendicular to the TI surface and are accompanied by a collapse of the minigap governed by the Thouless energy (depicted in Fig. 4a). They share many of the properties of zero bias anomalies observed in spectroscopic studies of nanowires coupled to superconducting leads [11–15]. While such studies were interpreted in terms of Majorana fermions, here we are more cautious. For example, weak anti-localization can also generate low energy resonances due to coherence between electron-hole trajectories that repeatedly impinge upon the superconductor-semiconductor interface [31]. Although originally proposed to describe diffusive semiconductors, such trajectories can exist in ballistic cavities due to multiple reflections off the boundary opposite of the superconductor-semiconductor interface [32]. In this respect, this phenomenon is similar to the de Gennes-Saint-James resonances but is restricted to near zero energy.

It has been pointed out that weak anti-localization in superconductor-semiconductor devices could survive in the presence of broken time-reversal symmetry, leading to low energy anomalies that are nearly identical in appearance to those attributed to Majorana fermions [33]. The persistence of the de Gennes-Saint-James resonances in our devices with magnetic field strongly suggests that the analogous trajectories for weak anti-localization can also remain phase coherent. This is in contrast to the previous assumption in the nanowire experiments that the large magnetic field would suppress weak anti-localization [11–15]. We note that while Refs. [34] and [35] explored non-topological origins of zero bias anomalies in quantum dots coupled to superconducting leads, here we extend the experimental analysis to

the limit of both ballistic transport and large coupling between the semiconductor segment and the metallic lead.

While the resonances in Fig. 3a might represent precursors to the low energy Andreev bound states that are predicted to form around the vortices of topological superconductors [2], further work is required to confirm the existence of Majorana bound states. Fortunately, our results demonstrate that it is feasible to construct Fabry-Perot interferometers on the surface of a topological insulator [4–6]. By flowing current through chiral edge channels formed at domain walls, one can probe the Z_2 interference of paths that enclose an even or odd number of vortices with Majorana fermions. Because the observed Fabry-Perot oscillations are robust after multiple fabrication steps and in the presence of large magnetic fields, our findings pave the way for not only interferometric probes of Majorana fermions but also more general studies of phase coherent transport in solid-state systems.

METHODS

Single crystals of Bi_2Se_3 were grown by melting a mixture of pure Bi and Se in a stoichiometric ratio of 1.9975:3 (Bi:Se) in a vacuum quartz tube at 800 °C. Thin flakes (7-20 nm) of Bi_2Se_3 were exfoliated onto silicon substrates covered by a 300 nm thick SiO_2 layer. Such thin flakes typically have a 2D carrier density of $N_{2D} \approx 10^{13} - 10^{14} \text{ cm}^{-2}$ and low temperature mobility $\mu \approx 10^2 - 10^3 \text{ cm}^2/\text{V-s}$. Weak anti-localization measurements give typical phase-coherence lengths of $\ell_\phi = 300 - 1000 \text{ nm}$ at 10 mK. Superconducting leads were defined by conventional e-beam lithography and a subsequent DC sputtering of 50 nm of Nb at room temperature. Tunnel junctions of $\text{Au}/\text{Al}_2\text{O}_3/\text{Nb}$ reveal a superconducting gap of $\Delta = 1.5 \text{ meV}$ for our Nb films immediately after sputtering; in top gated TI-Nb devices, the inverse proximity effect and additional nanofabrication processing will likely reduce the gap below this pristine value. Normal metal leads were deposited through e-beam evaporation of 5 nm of Ti and 50 nm of Au. Brief Ar ion milling is employed before metallization *in situ* to ensure good contact between the Bi_2Se_3 and the leads. Typical Nb-Au lead separation is 100-250 nm. Applying a bias to the silicon substrate permits back gating. A top gate may be created by covering the sample with 30 nm of alumina via ALD and deposition of Ti/Au over the exposed Bi_2Se_3 . The devices were thermally anchored to the mixing chamber of a cryogen-free dilution refrigerator equipped with a vector magnet and filtered wiring. We

perform low frequency transport measurements with standard lockin techniques, typically with a 10 nA AC excitation at $f = 73$ Hz. Unless stated otherwise, all measurements were performed at a base mixing chamber temperature of 20 mK.

ACKNOWLEDGEMENTS

We acknowledge helpful discussions with Rudro Biswas, Liang Fu, Pouyan Ghaemi, Taylor Hughes, and Shu-Ping Lee. C.K., A.D.K.F., and D.J.V.H. acknowledge funding by Microsoft Project Q. Y.S.H. acknowledges support from National Science Foundation grant DMR-12-55607. Device fabrication was carried out in the MRL Central Facilities (partially supported by the DOE under DE-FG02-07ER46453 and DE-FG02-07ER46471).

CONTRIBUTIONS

Y.S.H. grew the bismuth selenide crystals. A.D.K.F. and C.K. fabricated the devices and performed the measurements. A.D.K.F., C.K., and D.J.V.H. analyzed the data and wrote the manuscript.

COMPETING FINANCIAL INTERESTS

The authors report no competing financial interests.

-
- [1] M. Z. Hasan and C. L. Kane, “*Colloquium* : Topological insulators,” Rev. Mod. Phys. **82**, 3045–3067 (2010).
 - [2] Liang Fu and C. L. Kane, “Superconducting Proximity Effect and Majorana Fermions at the Surface of a Topological Insulator,” Phys. Rev. Lett. **100**, 096407 (2008).
 - [3] Chetan Nayak, Steven H. Simon, Ady Stern, Michael Freedman, and Sankar Das Sarma, “Non-Abelian anyons and topological quantum computation,” Rev. Mod. Phys. **80**, 1083–1159 (2008).
 - [4] Liang Fu and C. L. Kane, “Probing Neutral Majorana Fermion Edge Modes with Charge Transport,” Phys. Rev. Lett. **102**, 216403 (2009).

- [5] A. R. Akhmerov, Johan Nilsson, and C. W. J. Beenakker, “Electrically Detected Interferometry of Majorana Fermions in a Topological Insulator,” *Phys. Rev. Lett.* **102**, 216404 (2009).
- [6] K. T. Law, Patrick A. Lee, and T. K. Ng, “Majorana Fermion Induced Resonant Andreev Reflection,” *Phys. Rev. Lett.* **103**, 237001 (2009).
- [7] J. Alicea, “New directions in the pursuit of Majorana fermions in solid state systems,” *Rep. Prog. Phys.* **75**, 076501 (2012).
- [8] C.W.J. Beenakker, “Search for Majorana fermions in superconductors,” *Annu. Rev. Con. Mat. Phys.* **4**, 113 (2013).
- [9] P.G. de Gennes and D. Saint-James, “Elementary excitations in the vicinity of a normal metal-superconducting metal contact,” *Phys. Lett.* **4**, 151 (1963).
- [10] J. M. Rowell and W. L. McMillan, “Electron Interference in a Normal Metal Induced by Superconducting Contracts,” *Phys. Rev. Lett.* **16**, 453–456 (1966).
- [11] V. Mourik, K. Zuo, S.M. Frolov, S.R. Plissard, E.P.A.M. Bakkers, and L.P. Kouwenhoven, “Signatures of Majorana Fermions in Hybrid Superconductor-Semiconductor Nanowire Devices,” *Science* **336**, 1003–1007 (2012).
- [12] M. T. Deng, C. L. Yu, G. Y. Huang, M. Larsson, P. Caroff, and H. Q. Xu, “Anomalous Zero-Bias Conductance Peak in a Nb-InSb Nanowire-Nb Hybrid Device,” *Nano Letters* **12**, 6414 (2012).
- [13] A. Das, Y. Ronen, Y. Most, Y. Oreg, M. Heiblum, and H. Shtrikman, “Zero-bias peaks and splitting in an Al-InAs nanowire topological superconductor as a signature of Majorana fermions,” *Nature Phys.* **8**, 887 (2012).
- [14] A. D. K. Finck, D. J. Van Harlingen, P. K. Mohseni, K. Jung, and X. Li, “Anomalous Modulation of a Zero-Bias Peak in a Hybrid Nanowire-Superconductor Device,” *Phys. Rev. Lett.* **110**, 126406 (2013).
- [15] H. O. H. Churchill, V. Fatemi, K. Grove-Rasmussen, M. T. Deng, P. Caroff, H. Q. Xu, and C. M. Marcus, “Superconductor-nanowire devices from tunneling to the multichannel regime: Zero-bias oscillations and magnetoconductance crossover,” *Phys. Rev. B* **87**, 241401 (2013).
- [16] Wenjie Liang, Marc Bockrath, Dolores Bozovic, Jason H. Hafner, M. Tinkham, and Hongkun Park, “Fabry - Perot interference in a nanotube electron waveguide,” *Nature* **411**, 665 (2001).
- [17] Andrey V. Kretinin, Ronit Popovitz-Biro, Diana Mahalu, and Hadas Shtrikman, “Multimode Fabry-Perot Conductance Oscillations in Suspended Stacking-Faults-Free InAs Nanowires,”

- Nano Letters **10**, 3439–3445 (2010).
- [18] F. Miao, S. Wijeratne, Y. Zhang, U. C. Coskun, W. Bao, and C. N. Lau, “Phase-Coherent Transport in Graphene Quantum Billiards,” *Science* **317**, 1530–1533 (2007).
 - [19] G. E. Blonder, M. Tinkham, and T. M. Klapwijk, “Transition from metallic to tunneling regimes in superconducting microconstrictions: Excess current, charge imbalance, and super-current conversion,” *Phys. Rev. B* **25**, 4515–4532 (1982).
 - [20] Fan Yang, Yue Ding, Fanming Qu, Jie Shen, Jun Chen, Zhongchao Wei, Zhongqing Ji, Guang-tong Liu, Jie Fan, Changli Yang, Tao Xiang, and Li Lu, “Proximity effect at superconducting Sn-Bi₂Se₃ interface,” *Phys. Rev. B* **85**, 104508 (2012).
 - [21] G. Koren and T. Kirzhner, “Zero-energy bound states in tunneling conductance spectra at the interface of an *s*-wave superconductor and a topological insulator in NbN/Bi₂Se₃/Au thin-film junctions,” *Phys. Rev. B* **86**, 144508 (2012).
 - [22] S.N. Artemenko, A.F. Volkov, and A.V. Zaitsev, “On the excess current in microbridges s-c-s and s-c-n,” *Solid State Communications* **30**, 771 – 773 (1979).
 - [23] Yuli V. Nazarov and T. H. Stoof, “Diffusive Conductors as Andreev Interferometers,” *Phys. Rev. Lett.* **76**, 823–826 (1996).
 - [24] A. A. Golubov, F. K. Wilhelm, and A. D. Zaikin, “Coherent charge transport in metallic proximity structures,” *Phys. Rev. B* **55**, 1123–1137 (1997).
 - [25] James G. Analytis, Ross D. McDonald, Scott C. Riggs, Jiun-Haw Chu, G. S. Boebinger, and Ian R. Fisher, “Two-dimensional surface state in the quantum limit of a topological insulator,” *Nat. Phys.* **6**, 960 (2010).
 - [26] Timothy H. Hsieh and Liang Fu, “Majorana Fermions and Exotic Surface Andreev Bound States in Topological Superconductors: Application to Cu_xBi₂Se₃,” *Phys. Rev. Lett.* **108**, 107005 (2012).
 - [27] Satoshi Sasaki, M. Kriener, Kouji Segawa, Keiji Yada, Yukio Tanaka, Masatoshi Sato, and Yoichi Ando, “Topological Superconductivity in Cu_xBi₂Se₃,” *Phys. Rev. Lett.* **107**, 217001 (2011).
 - [28] J. G. Checkelsky, Y. S. Hor, R. J. Cava, and N. P. Ong, “Bulk Band Gap and Surface State Conduction Observed in Voltage-Tuned Crystals of the Topological Insulator Bi₂Se₃,” *Phys. Rev. Lett.* **106**, 196801 (2011).

- [29] Jien Cao, Qian Wang, and Hongjie Dai, “Electron transport in very clean, as-grown suspended carbon nanotubes,” *Nat. Mater.* **4**, 745 (2005).
- [30] Andrei V. Shytov, Mark S. Rudner, and Leonid S. Levitov, “Klein Backscattering and Fabry-Pérot Interference in Graphene Heterojunctions,” *Phys. Rev. Lett.* **101**, 156804 (2008).
- [31] B. J. van Wees, P. de Vries, P. Magnée, and T. M. Klapwijk, “Excess conductance of superconductor-semiconductor interfaces due to phase conjugation between electrons and holes,” *Phys. Rev. Lett.* **69**, 510–513 (1992).
- [32] M. Schechter, Y. Imry, and Y. Levinson, “Reflectionless tunneling in ballistic normal–metal–superconductor junctions,” *Phys. Rev. B* **64**, 224513 (2001).
- [33] D.I. Pikulin, J.P. Dahlhaus, M. Wimmer, H. Schomerus, and C.W.J. Beenakker, “A zero-voltage conductance peak from weak antilocalization in a Majorana nanowire,” *New Journal of Physics* **14**, 125011 (2012).
- [34] Eduardo J. H. Lee, Xiaocheng Jiang, Ramón Aguado, Georgios Katsaros, Charles M. Lieber, and Silvano De Franceschi, “Zero-Bias Anomaly in a Nanowire Quantum Dot Coupled to Superconductors,” *Phys. Rev. Lett.* **109**, 186802 (2012).
- [35] Eduardo J.H. Lee, Xiaocheng Jiang, Manuel Houzet, Ramón Aguado, Charles M. Lieber, and Silvano De Franceschi, “Spin-resolved Andreev levels and parity crossings in hybrid superconductor-semiconductor nano structures,” *Nature Nanotechnology* **9**, 79 (2014).

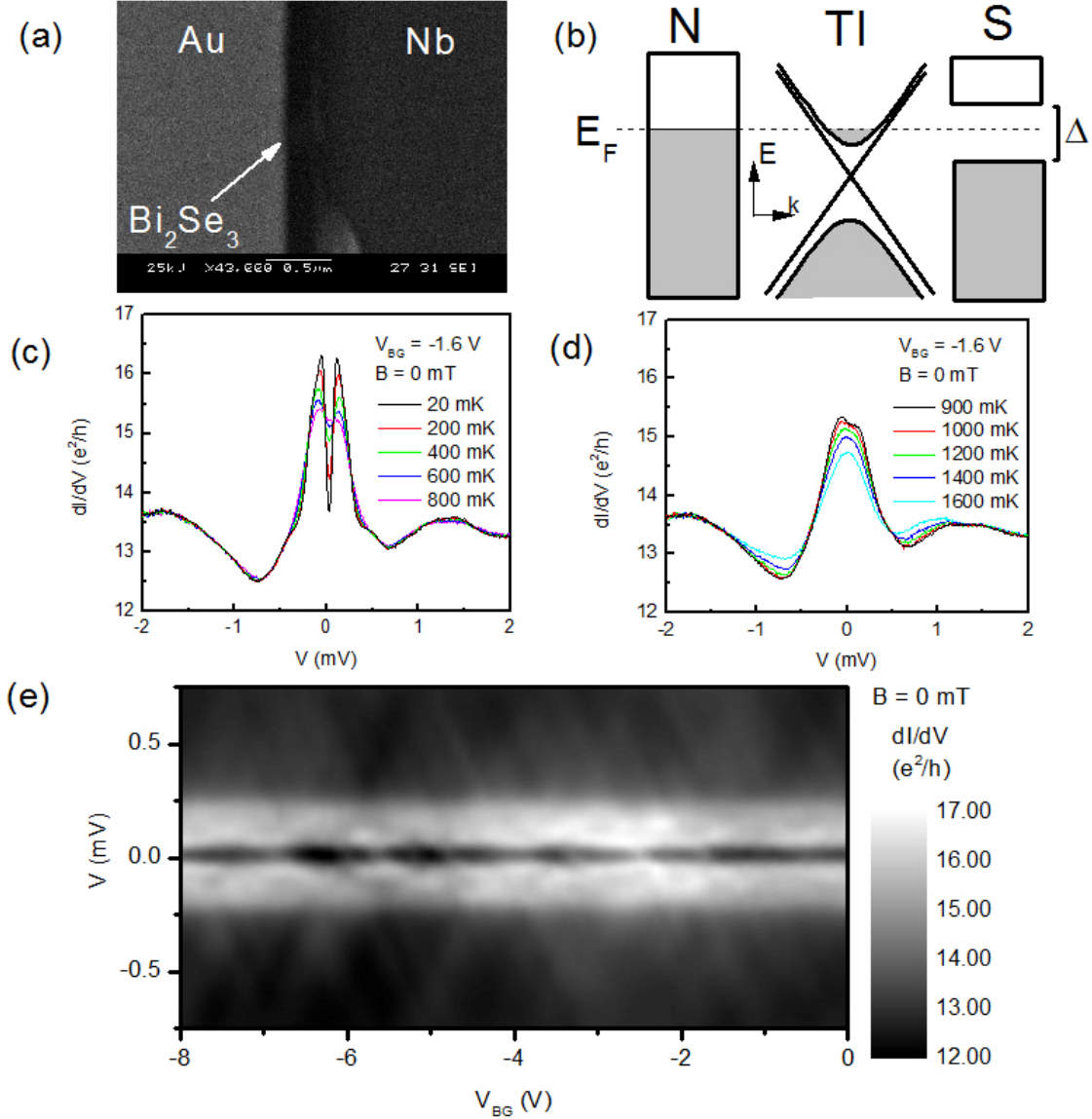


FIG. 1. (a) SEM of N-TI-S device. The barely visible Bi₂Se₃ segment originally consisted of two adjacent nanoribbons that are each 9 nm thick and 250 nm wide, but subsequent AFM imaging after measurements revealed only one nanoribbon remaining. Separation between N and S leads is $L = 230$ nm. (b) Energy diagram for the three materials in the device. The TI (whose dispersion relation is depicted with both gapless helical surface states and gapped trivial states) is sandwiched between a compressible normal metal and a superconductor with an energy gap Δ . (c) I-Vs vs temperature at zero field. At low bias, the conductance is suppressed due to the re-entrant resistance effect. (d) I-Vs at zero field and elevated temperature. When the temperature exceeds the Thouless energy, the low bias conductance suppression is replaced by a broad conductance peak. (e) Stability plot at zero field at 20 mK.

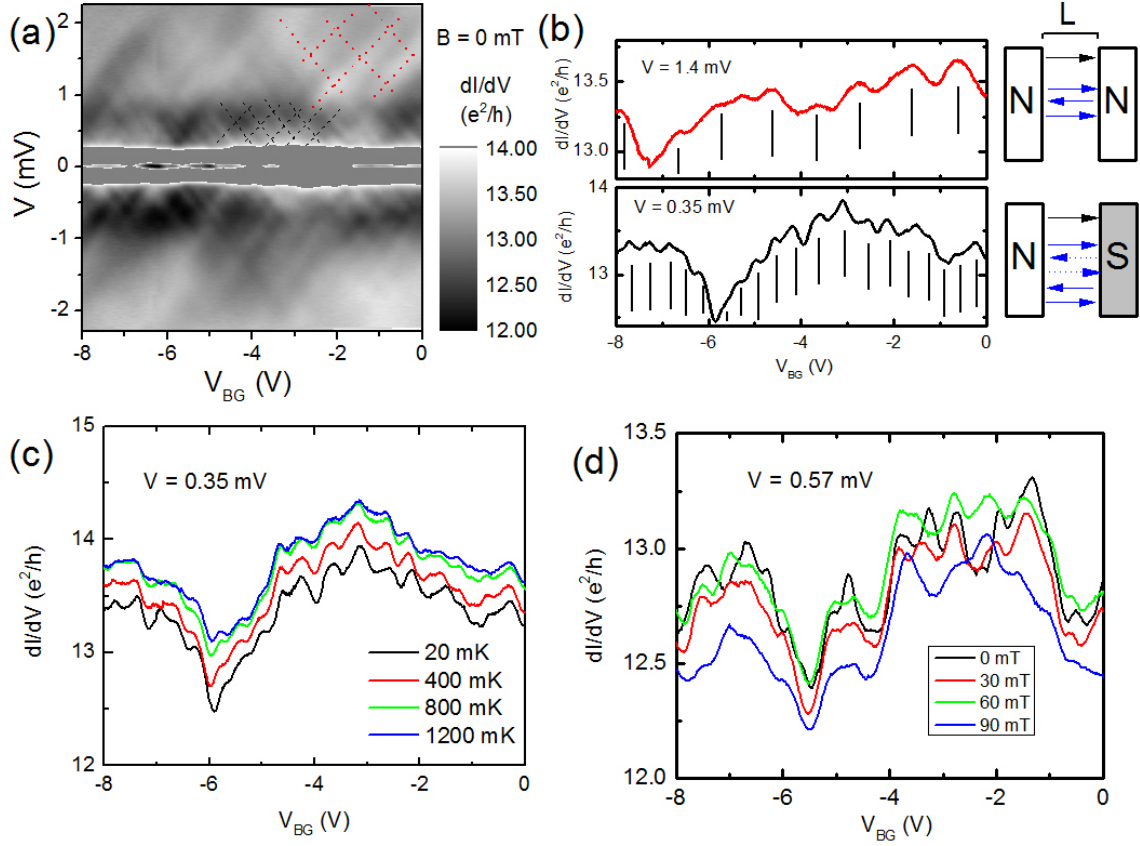


FIG. 2. (a) Stability plot accentuating the high bias features. Red dotted lines indicate the checkerboard pattern for conventional Fabry-Perot oscillation at high bias. Black dashed lines follow the low bias features for de Gennes-Saint-James resonances. (b) Differential conductance vs back gate bias for two different values of source-drain bias V . The red trace shows the Fabry-Perot oscillations at high bias, with period $\Delta V_{BG} \approx 1$ V. The black trace shows the low energy de Gennes-Saint-James resonances with period $\Delta V_{BG} \approx 0.5$ V. The cartoons on the right symbolize the two sets of particle trajectories for Fabry-Perot resonances (with electrons only) and de Gennes-Saint-James resonances (mixture of holes and electrons). (c) Temperature dependence of de Gennes-Saint-James oscillations at zero field. (d) Magnetic field dependence of de Gennes-Saint-James oscillations. These features persist up to at least 90 mT.

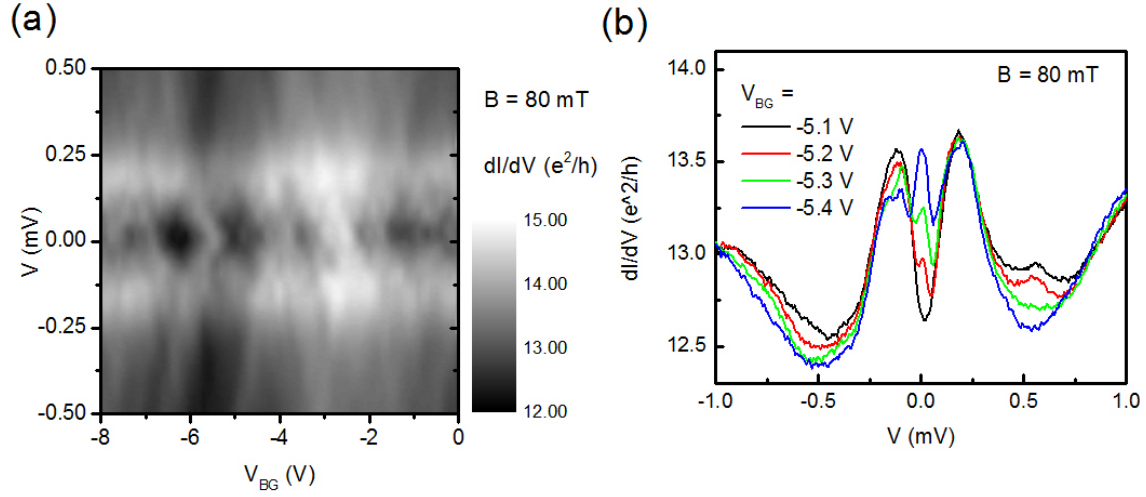


FIG. 3. (a) Stability plot at $B = 80$ mT, with intricate low energy resonances. (d) Example I-Vs at 80 mT, showing evolution of zero bias peak near $V_{BG} = -5.4$ V.

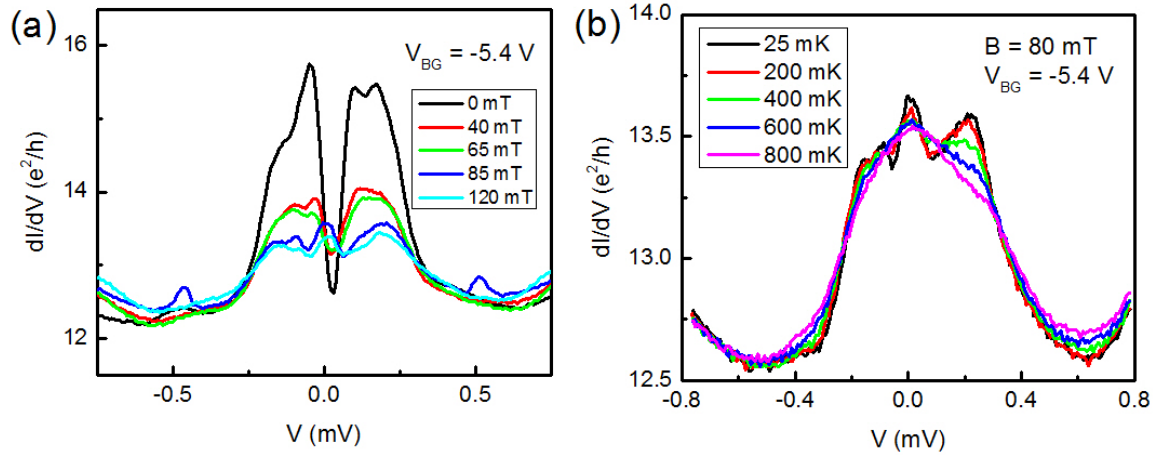


FIG. 4. (a) Magnetic field evolution of zero bias peak at $V_{BG} = -5.4$ V. Peak appears beyond 65 mT and remains for up to $B = 120$ mT. No such peak is present at zero field or when an in-plane field is applied perpendicular to current flow. (b) Temperature dependence of zero bias peak at 80 mT. Thermal fluctuations cause the peak to broaden and merge with background.

Supplementary Materials: Phase Coherence and Andreev Reflection in Topological Insulator Devices

A.D.K. Finck^{1*}, C. Kurter^{1*}, Y.S. Hor², D.J. Van Harlingen¹

¹*Department of Physics and Materials Research Laboratory,*

University of Illinois at Urbana-Champaign, Urbana, Illinois 61801

²*Department of Physics, Missouri University of Science and Technology, Rolla, MO 65409*

** These authors contributed equally to the work.*

(Dated: March 25, 2014)

To buttress the claims in the main text, here we present data from additional samples that show the same behavior as the primary sample. This includes observations of the re-entrant resistance effect, Fabry-Perot oscillations, and low-energy resonances that emerge in the presence of an out-of-plane magnetic field.

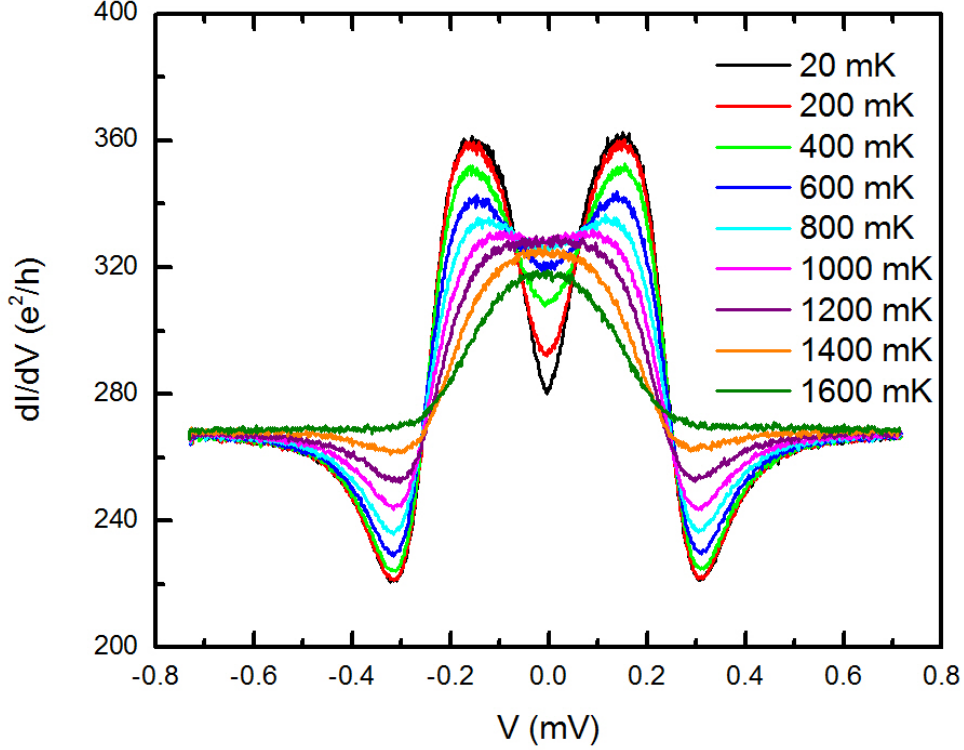


FIG. S1. Conductance vs source-drain bias V for Sample T3-V at various temperatures.

I. ADDITIONAL EVIDENCE FOR RE-ENTRANT RESISTANCE EFFECT

Sample T3-V consisted of a 15 nm thick flake of Bi_2Se_3 with one gold lead and one niobium lead, separated by $L = 135$ nm. The device was relatively highly conducting (normal state $G \approx 270 e^2/h$), possibly due to larger bulk conductance. As shown in Fig. S1, this device also displayed signs of the re-entrant resistance effect. Because the lead separation is smaller in this device than in the sample described in the main text, the Thouless energy $E_T = \hbar D/L^2$ is correspondingly larger and the suppression in conductance occurs over a wider range in source-drain bias V . This sample possessed a top gate, but the normal state resistance was relatively affected by a top gate bias. Similar behavior occurred in other highly conducting samples, none of which displayed any clear signs of Fabry-Perot oscillations. This supports the assertion of greater bulk contribution to the conductance in these samples as well as demonstrates that the gate-tuned Fabry-Perot oscillations originate from surface states.

II. ADDITIONAL FABRY-PEROT OSCILLATIONS

Sample T3-VII consisted of a 7 nm thick flake of Bi_2Se_3 with one gold lead and one niobium lead, separated by $L = 95$ nm. The chemical potential is tuned by a top gate separated from the sample by 30 nm of Al_2O_3 . This type of gating is susceptible to charge noise. Nonetheless, we were able to resolve both de Gennes-Saint-James resonances at low energies and conventional Fabry-Perot oscillations at energies beyond the niobium gap. In Fig. S2a, we show an example of a stability plot for this device, with the location of the de Gennes-Saint-James resonances indicated by dashed lines. Note that the geometric resonances can lead to a zero bias peak in conductance. Similar behavior was observed at zero field, but the resonances are more apparent in the 50 mT data set due to less charge noise. In Fig. S2b, we show top gate sweeps of conductance at zero field for two different source-drain biases to highlight the two types of geometric resonances. Charge noise is apparent in this measurement in the form of discontinuities in the traces. At source-drain biases beyond the niobium superconducting gap (≈ 1 mV), we observe conventional Fabry-Perot oscillations with half the frequency as the low bias oscillations.

From the slopes of the features in the stability plot (Fig. S2a), we observe that a 1 V change in top gate bias shifts the Fermi energy by 5.7 mV. The Fabry-Perot oscillations at high V possess a periodicity of $\Delta V_{TG} = 0.4$ V; this is equivalent to a periodicity in Fermi energy of $\Delta E = 2.3$ mV. This is consistent with the prediction that ΔE for this device should be larger than that of the device in the main text by the ratio of $(235 \text{ nm}) / (95 \text{ nm}) = 2.47$, based on the formula $\Delta E = \hbar v_F / L$.

III. ADDITIONAL EVIDENCE FOR LOW ENERGY RESONANCES

Sample N5-VI consisted of a 17 nm thick and 250 nm wide flake of Bi_2Se_3 with a narrow (100 nm) gold lead in between two niobium leads. The gold lead was separated by $L \approx 100$ nm from either niobium lead. The two niobium leads are connected by a superconducting loop, enabling a phase-bias to be applied to the two superconducting leads. However, the conductance of the device showed no signs of phase-sensitivity. The device responded to large magnetic fields in ways similar to devices with only one superconducting lead.

At zero magnetic field, Sample N5-VI displayed signs of the re-entrant resistance effect.

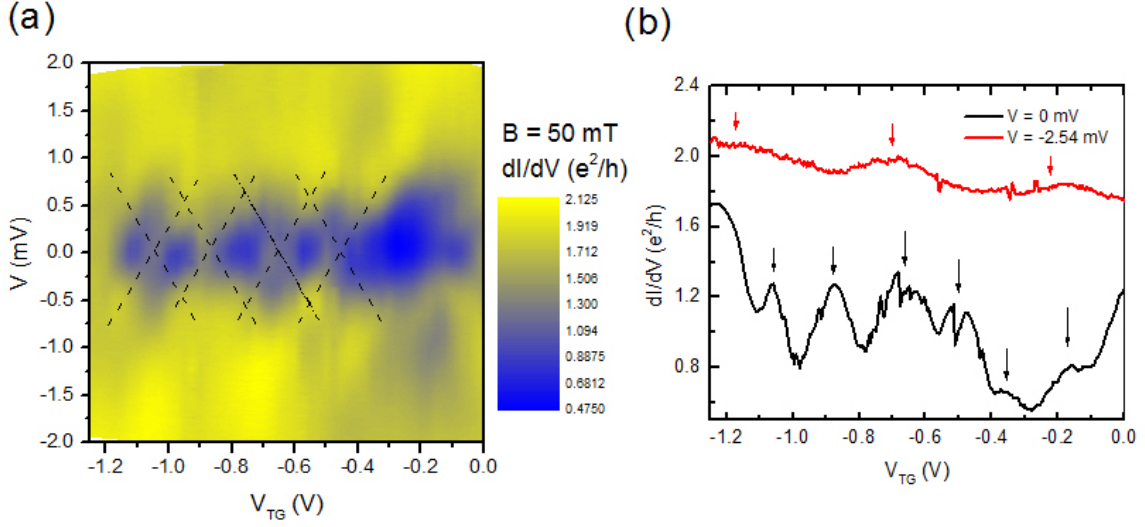


FIG. S2. (a) Stability plot at 50 mT for Sample T3-VII. Dashed lines indicate low-energy de Gennes-Saint-James resonances. (b) Top gate sweeps at 0 mT for two difference source-drain biases V . Arrows indicate locations of maximal constructive interference.

In Fig. S3a, we show a stability plot at zero magnetic field. Note the lack of sharp features. Both periodic Fabry-Perot oscillations and aperiodic universal conductance fluctuations were observed, as seen in the back gate trace in Fig. S3b. A checkerboard pattern for Fabry-Perot oscillations emerges after numerical differentiation of the data in Fig. S3a.

In large magnetic fields ($B > 30$ mT), a number of gate-tunable, low-energy resonances emerge, similar to the anomalies seen in the sample described in the main text. A stability plot in Fig. S3c shows such resonances at 39.6 mT, with sample $I - V$ s in Fig. S3d. The low-energy resonances take the form of narrow shoulders in the $I - V$ s of height $\approx e^2/h$. The resonances continue to evolve with field, as seen in Fig. S3e. Here, a zero bias peak can emerge, as plotted in Fig. S3f. The peak is narrow (FWHM ≈ 50 μ V) and has a height of $\approx e^2/h$. We emphasize that no such peak is seen at zero field at this gate bias. In-plane magnetic fields have no effect on transport signatures of this device up to 100 mT.

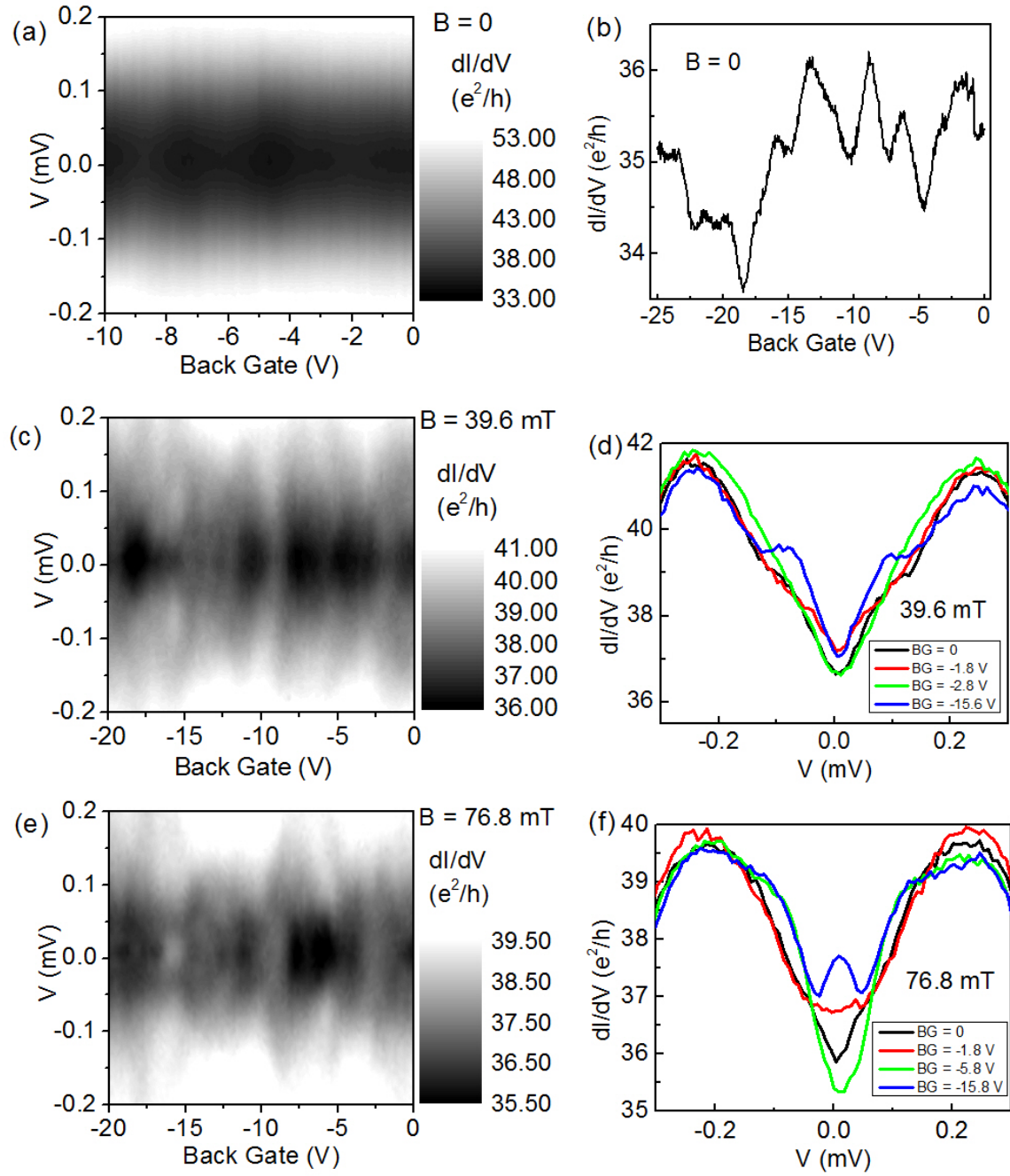


FIG. S3. Sample N5-VI (a) Stability plot at zero field, with no resonances. (b) Back gate sweep at zero field, with both Fabry-Perot resonances and universal conductance fluctuations. (c) Stability plot at 39.6 mT, showing gate-tunable features. (d) Sample $I - V$ s at 39.6 mT. (e) Stability plot at 76.8 mT. (f) Sample $I - V$ s at 76.8 mT, including zero bias peak at $V_{BG} = -15.8$ V.